Publishing House
AKAPIT

COMPUTER METHODS IN MATERIALS SCIENCE
Informatyka w Technologii Materiałów

Vol. 9, 2009, No. 2

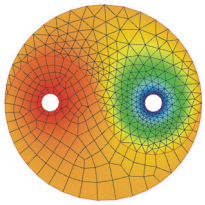

AN IMPLICIT NUMERICAL INTEGRATION ALGORITHM FOR BAI & WIERZBICKI (2007) ELASTO-PLASTIC MODEL

LUCIVAL MALCHER, FRANCISCO M. ANDRADE PIRES, JOSÉ M.A. CÉSAR DE SÁ, FILIPE X.C. ANDRADE

Department of Mechanical Engineering, Faculty of Engineering, University of Porto
Rua Dr. Roberto Frias, Porto 4200-465, Portugal
Corresponding Author: lucival.malcher@fe.up.pt; (L. Malcher)

Abstract

This contribution describes an implicit algorithm for numerical integration of a recently proposed model for metal plasticity and fracture [2]. The constitutive equations of the material model critically include both the effect of pressure through the triaxiality ratio and the effect of third deviatoric stress invariant through the lode angle in the description of material. These effects are directly introduced on the hardening rule of the material. The theoretical basis of the material model is presented in the first part of the paper. Then, the necessary steps required to implement the model within an implicit quasi-static finite element environment are discussed. In particular, the stress update procedure, which is based on the so-called operator split concept resulting in the standard elastic predictor/return mapping algorithm, and the computation of tangent matrix consistent with the stress update are described. Finally, the simulation of a flat grooved specimen subjected to tension [1] is presented to illustrate the robustness and efficiency of the proposed algorithm.

Key words: finite element method, elasto-plastic model, hydrostatic pressure sensitivity, lode angle dependence

1. INTRODUCTION

One of the most commonly used models to describe the behavior of metals is the von Mises model. According to this model, plastic yielding begins when the second invariant of the deviatoric stress tensor, J_2, reaches a critical value. The pressure component of the stress tensor does not take part in the definition of yielding and consequently the model can be regarded as "pressure-insensitive" [5]. Another feature of the model, when compared to other material models, is that it is also independent of the third invariant of the deviatoric stress tensor. Both parameters have got a well known influence on the yield surface [8]. The level of hydrostatic is responsible for controlling the size of the yield surface and the third invariant is responsible for the shape of the yield surface [1].

The importance of the hydrostatic stress and lode angle has been recognized by several authors and introduced into the constitutive description of some materials such as soils, rocks and concrete [2,8]. In the case of ductile materials, which are addressed in this paper, many researchers have conducted extensive experimental studies. Richmond and Spitzing [6] were among of the first researchers to investigate the effect of pressure on yielding of aluminum alloys.

Ductile fracture is a local phenomenon and the state of stress and strain, at the expected fracture location, must be determined with accuracy. Fracture initiation is often preceded by large plastic deformation and there are considerable stress and strain gradients around the point of fracture. In this case, the J_2 theory is not accurate enough and more refined plasticity models have to be introduced.

ISSN 1641-8581

The determination of an adequate shape of the yield surface has become an important issue in sheet metal forming. In this case, the von Mises plane stress ellipse does not lead to a correct prediction of necking instability. To overcome some of the previous limitations, Bai & Wierzbicki [2] have proposed a model that includes both the effect of pressure and the third invariant on the evolution of plastic flow.

Preliminaries

For the sake of completeness and notation clarity, we will briefly summarize some fundamental relations commonly used in plasticity**.** The stress tensor can be split in two components: an hydrostatic and a deviatoric component, which can be represented as:

$$\underline{\boldsymbol{\sigma}} = \underline{\boldsymbol{S}} + p\underline{\boldsymbol{I}} \tag{1}$$

The strain tensor can also be split in two components:

$$\underline{\boldsymbol{\varepsilon}}^e = \underline{\boldsymbol{\varepsilon}}_d^e + \varepsilon_v^e \underline{\boldsymbol{I}} \tag{2}$$

where, $\underline{\boldsymbol{\sigma}}$ is the stress tensor, $\underline{\boldsymbol{S}} = \underline{\boldsymbol{\sigma}} - p\underline{\boldsymbol{I}} = 2G\underline{\boldsymbol{\varepsilon}}_d^e$ is the deviatoric stress tensor, $p = \frac{1}{3}tr(\underline{\boldsymbol{\sigma}}) = K\varepsilon_v^e$ represents the pressure or hydrostatic stress, $\underline{\boldsymbol{\varepsilon}}^e$ is the elastic strain tensor, $\underline{\boldsymbol{\varepsilon}}_d^e$ is the deviatoric strain tensor and ε_v^e represents the volumetric strain. The constants G and K are, respectively, the shear modulus and the bulk modulus. We can also define the equivalent stress, which is a function of the second invariant of deviatoric stress tensor, as:

$$q = \sqrt{3J_2} = \sqrt{\frac{3}{2}\,\underline{\boldsymbol{S}} : \underline{\boldsymbol{S}}} = \sqrt{\frac{3}{2}}\,\|\underline{\boldsymbol{S}}\| \tag{3}$$

where, q is the equivalent stress, J_2 is the second invariant of the deviatoric stress and $\|\underline{\boldsymbol{S}}\|$ represents the norm of the deviatoric stress tensor.

The third invariant is a scalar quantity that is obtained by computing the determinant of the deviatoric stress tensor, denoted by $J_3 = det(\underline{\boldsymbol{S}})$. Alternatively, the third invariant can be expressed by:

$$r = \left[\frac{27}{2}J_3\right]^{1/3} = \left[\frac{27}{2}\,det(\underline{\boldsymbol{S}})\right]^{1/3} \tag{4}$$

The influence of pressure on the von Mises elasto-plastic model can be introduced through the triaxiality ratio which is a dimensionless hydrostatic stress. The triaxiality ratio is defined as the ratio between the pressure and the equivalent stress:

$$\eta = \frac{p}{q} \tag{5}$$

The third invariant of the deviatoric stress tensor can be normalized and related with the so-called lode angle through the expression:

$$\xi = \left(\frac{r}{q}\right)^3 = \frac{27}{2}.\frac{det(\underline{\boldsymbol{S}})}{q^3} = \cos(3\theta) \tag{6}$$

where, ξ is the normalized third invariant and θ is the lode angle. Since the range of the lode angle is $0 \le \theta \le \pi/3$, the range of ξ has to be $-1 \le \xi \le 1$. The lode angle can also be normalized by:

$$\bar{\theta} = 1 - \frac{6\theta}{\pi} = 1 - \frac{2}{\pi}arccos(\xi) \tag{7}$$

where, $\bar{\theta}$ is the normalized lode angle. The range of $\bar{\theta}$ is $-1 \le \bar{\theta} \le 1$. The parameter $\bar{\theta}$ will be called the lode angle parameter hereinafter.

2. THE BAI & WIERZBICKI YIELD FUNCTION

Bai & Wierzbicki [2] have proposed an elasto-plastic model that includes both the effect of pressure (through the triaxiality ratio) and the effect of the third invariant of the deviatoric stress tensor (through the lode angle). These effects are introduced by redefining the hardening rule. While in the classic von Mises model, the hardening rule is only a function of the accumulated plastic strain, $\sigma_y(\bar{\varepsilon}^p)$, in Bai & Wierzbicki´s model the hardening rule is a function of the accumulated plastic strain, the triaxiality ratio and the parameter $\mu(\theta)$, which is a function of the load angle. The hardening rule is rewritten as:

$$\sigma_y(\bar{\varepsilon}^p, \eta, \gamma) = \sigma_y(\bar{\varepsilon}^p).\left[1 - C_\eta(\eta - \eta_0)\right].$$
$$\left[C_\theta^s + (C_\theta^{ax} - C_\theta^s)\left(\mu - \frac{\mu^{m+1}}{m+1}\right)\right] \tag{8}$$

where, $\sigma_y(\bar{\varepsilon}^p)$ is the material strain hardening function, $C_\eta, C_\theta^s, C_\theta^{ax}$, and m are experimental parameters, η_0 is the reference value of the triaxiality ratio and $\mu(\theta)$ is a parameter defined as a function of the lode angle:

$$\mu(\theta) = \frac{\cos(\pi/6)}{1 - \cos(\pi/6)}\left[\frac{1}{\cos(\theta - \pi/6)} - 1\right] =$$
$$\frac{\cos(\pi/6)}{1-\cos(\pi/6)}.\left[\sec(\theta - \pi/6) - 1\right] \tag{9}$$

The effect of the triaxiality ratio and load angle are included on the hardening rule through the parameters $A(\eta) = \left[1 - C_\eta(\eta - \eta_0)\right]$ and $B(\mu) = \left[C_\theta^s + (C_\theta^{ax} - C_\theta^s)\left(\mu - \frac{\mu^{m+1}}{m+1}\right)\right]$, respectively. The new yield criterion is simply obtained by replacing

the standard hardening rule $\sigma_y(\bar{\varepsilon}^p)$ by $\sigma_y(\bar{\varepsilon}^p, \eta, \mu)$ on the von Mises yield function, which can be represented by Φ, as:

$$\Phi = q - \sigma_y(\bar{\varepsilon}^p).\left[1 - C_\eta(\eta - \eta_0)\right].$$
$$\left[C_\theta^s + (C_\theta^{ax} - C_\theta^s)\left(\mu - \frac{\mu^{m+1}}{m+1}\right)\right] \qquad (10)$$

In order to understand the above yield function, let us analyze the influence of some experimental parameters $(C_\eta, C_\theta^s, C_\theta^{ax}, \eta_0, m)$ on the behavior of the model. The parameter C_η is a material constant that needs to be experimentally calibrated and that describes the effect of the hydrostatic pressure on the material plastic flow. If $C_\eta = 0$, the model loses the dependence of the triaxiality (and of the hydrostatic pressure) and recovers, as a limiting case, the behavior of the von Mises model.

The reference triaxiality, η_0, depends on both the type of load applied and the geometry of the specimen. For a smooth bar subjected to tension, η_0 takes the value equal to $1/3$, for a cylindrical specimen under compression η_0 is equal to $-1/3$ and for both torsion and shear tests η_0 is equal to 0. With regard to the third invariant effect, the experimental parameter C_θ^{ax} can assume one of two forms, according to the value of the normalized lode angle $\bar{\theta}$.

$$C_\theta^{ax} = \begin{cases} C_\theta^t \; for \; \bar{\theta} \geq 0 \\ C_\theta^c \; for \; \bar{\theta} < 0 \end{cases} \qquad (11)$$

The parameter C_θ^s also depends on the type of test. For example, if a smooth bar is used in a tensile test $C_\theta^t = 1$, if a torsion test $C_\theta^s = 1$, if a cylinder specimen is used in a compressive test $C_\theta^c = 1$. The convexity of the yield surface is controlled by the ratio of these parameters. The range of the parameter μ is between $0 \leq \mu \leq 1$. When $\mu = 0$ it corresponds to plane strain or shear condition, when $\mu = 1$ it corresponds to axisymmetric problem. The introduction of the term $\frac{\mu^{m+1}}{m+1}$ is done to ensure the smoothness of yield surface and its differentiability with respect to lode angle around $\mu = 1$.

3. NUMERICAL INTEGRATION ALGORITHM

An algorithm treatment of the model summarized in section 2 relies on the operator split methodology, which results in an elastic predictor/plastic corrector algorithm [4,7]. In the elastic predictor phase (obtained by freezing the plastic flow during the time interval $[t_n, t_{n+1}]$), values from the previous converged solution are used as initial conditions to evaluate the elastic trial state, i.e., the exact elastic solution.

If the yield condition is violated, the plastic corrector is initiated based on the Newton-Raphson procedure. The governing equations for one step of the Newton-Raphson iterative scheme are summarized in Box 1.

4. NUMERICAL EXAMPLE

This section presents an example to illustrate basic aspects of the proposed integration algorithm described previously. A tensile test of flat grooved plates, as shown in figure 1, is used to illustrate the numerical performance of the proposed algorithm within an implicit quasi-static finite element environment. The relative residual of the solution is presented to show the asymptotic convergence of the algorithm.

The specimen has been subjected to monotonic axial stretching and the numerical results are compared with experimental results reported by Bai *et al* [2]. The material properties including the pressure effect and lode dependence constants, adopted in the present analysis, are listed in table 1. These parameters were taken from Bai [1] for an aluminum alloy.

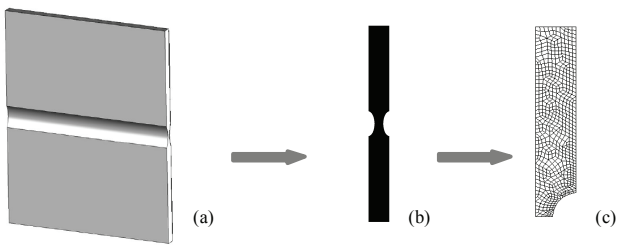

Fig. 1. *(a) Flat grooved specimen, thickness = 2.11 mm, groove radius = 1.59 mm, width = 50 mm, plate thickness = 5 mm. (b) a longitudinal section of the specimen and (c) Finite element mesh: 1981 nodes and 616 elements.*

Table 1. *Calibrated material properties of aluminum 2024-T351.*

Basic material properties			Pressure and lode constants	
Description	Symbol	Value	η_0	*1/3*
Density	ρ	2.7 10^3 Kg/m^3	C_η	0.009
Elastic Modulus	E	7.115 10^5 [MPa]	C_θ^t	1.0
Poisson´s ratio	v	0.3	C_θ^s	0.855
Initial yield stress	σy0	370 [MPa]	C_θ^c	0.90
Hardening curve	σy($\bar{\varepsilon}^p$)	908(0.0058+$\bar{\varepsilon}^p$)$^{0.1742}$ [MPa]	m	6

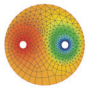

Box 1: *Fully implicit Elastic predictor/Return mapping algorithm.*

i) Evaluate the elastic trial state: Given the incremental strain $\Delta\varepsilon$ and the state variables at t_n.

$$\underline{\boldsymbol{\varepsilon}}^{e\,trial}_{n+1} = \underline{\boldsymbol{\varepsilon}}^{e}_{n} + \Delta\underline{\boldsymbol{\varepsilon}} \quad , \quad q^{trial}_{n+1} = \sqrt{\frac{3}{2}\,\underline{\boldsymbol{S}}^{trial}_{n+1} : \underline{\boldsymbol{S}}^{trial}_{n+1}} \quad , \quad \theta^{trial}_{n+1} = \frac{1}{3}arccos\left(\xi^{trial}_{n+1}\right)$$

$$\bar{\boldsymbol{\varepsilon}}^{p\,trial}_{n+1} = \bar{\boldsymbol{\varepsilon}}^{p}_{n} \quad , \quad \eta^{trial}_{n+1} = \frac{p^{trial}_{n+1}}{q^{trial}_{n+1}} \quad , \quad \mu^{trial}_{n+1} = \frac{\cos(\pi/6)}{1-\cos(\pi/6)}.\left[sec\left(\theta^{trial}_{n+1} - \pi/6\right) - 1\right]$$

$$p^{trial}_{n+1} = K\varepsilon^{e\,trial}_{v\,n+1} \quad , \quad r^{trial}_{n+1} = \left[\frac{27}{2}\det\left(\underline{\boldsymbol{S}}^{trial}_{n+1}\right)\right]^{1/3} \quad , \quad A^{trial}_{n+1} = \left[1 - C_\eta\left(\eta^{trial}_{n+1} - \eta_0\right)\right]$$

$$\underline{\boldsymbol{S}}^{trial}_{n+1} = 2G\underline{\boldsymbol{\varepsilon}}^{e\,trial}_{d\,n+1} \quad , \quad \xi^{trial}_{n+1} = \left(\frac{r^{trial}_{n+1}}{q^{trial}_{n+1}}\right)^3 \quad , \quad B^{trial}_{n+1} = \left[C^s_\theta + \left(C^{ax}_\theta - C^s_\theta\right)\left(\mu^{trial}_{n+1} - \frac{\mu^{trial\,m+1}_{n+1}}{m+1}\right)\right]$$

ii) Check plastic admissibility:

IF $\Phi = q^{trial}_{n+1} - \sigma_y\left(\bar{\varepsilon}^{p\,trial}_{n+1}\right).A^{trial}_{n+1}.B^{trial}_{n+1} \le 0$, THEN set $(\cdot)_{n+1} = (\cdot)^{trial}_{n+1}$ (elastic step)

iii) Return mapping (plastic step):

Solve the system of equations below for $\underline{\boldsymbol{\varepsilon}}^{e}_{n+1}$, $\Delta\gamma$ *and* $\bar{\varepsilon}^{p}_{n+1}$ *using Newton-Raphson method:*

$$\begin{Bmatrix} r_{\underline{\boldsymbol{\varepsilon}}^{e}_{n+1}} \\ r_{\Delta\gamma} \\ r_{\bar{\varepsilon}^{p}_{n+1}} \end{Bmatrix} = \begin{Bmatrix} \mathbf{0} \\ 0 \\ 0 \end{Bmatrix} <=> \begin{Bmatrix} \underline{\boldsymbol{\varepsilon}}^{e}_{n+1} - \underline{\boldsymbol{\varepsilon}}^{e\,trial}_{n+1} + \Delta\gamma.\boldsymbol{N}_{n+1} \\ q_{n+1} - \sigma_y(\bar{\varepsilon}^{p}_{n+1}).A_{n+1}.B_{n+1} \\ \bar{\varepsilon}^{p}_{n+1} - \bar{\varepsilon}^{p\,trial}_{n+1} - \Delta\gamma\sqrt{(*)} \end{Bmatrix} = \begin{Bmatrix} \mathbf{0} \\ 0 \\ 0 \end{Bmatrix}$$

$$(*) = \alpha^2_{n+1} + \lambda^2_{n+1}\frac{S^2_{n+1} : S^2_{n+1}}{S_{n+1} : S_{n+1}} + \frac{2.\beta^2_{n+1}}{9} + 3.\alpha^2_{n+1}.\lambda^2_{n+1}\frac{S_{n+1} : S^2_{n+1}}{S_{n+1} : S_{n+1}} + \frac{2.\lambda^2_{n+1}.\beta^2_{n+1}}{3.q_{n+1}}tr(S^2_{n+1})$$

GOTO Box 2

iv) Update the state variables:

$$\underline{\boldsymbol{\varepsilon}}^{e}_{d\,n+1} = \frac{1}{2G}\underline{\boldsymbol{S}}_{n+1} \quad , \quad \varepsilon^{e}_{v\,n+1} = \frac{1}{K}p_{n+1} \quad , \quad \underline{\boldsymbol{\varepsilon}}^{e}_{n+1} = \underline{\boldsymbol{\varepsilon}}^{e}_{d\,n+1} + \frac{1}{3}\varepsilon^{e}_{v\,n+1}\underline{\boldsymbol{I}} \quad , \quad \bar{\varepsilon}^{p}_{n+1} = \bar{\varepsilon}^{p}_{n} + \Delta\bar{\varepsilon}^{p}$$

v) Exit

where $r_{\underline{\boldsymbol{\varepsilon}}^{e}_{n+1}}$, $r_{\Delta\gamma}$ *and* $r_{\bar{\varepsilon}^{p}_{n+1}}$ *are the residual functions for each variable of the problem.* $\boldsymbol{N}_{n+1}$ *represents the flow vector and can be defined as:* $\boldsymbol{N} \equiv \frac{\partial\Phi}{\partial\underline{\sigma}} = \frac{3\alpha}{2q}\underline{\boldsymbol{S}} + \frac{3\lambda}{2q}\underline{\boldsymbol{S}}^2 + \frac{\beta}{3}\underline{\boldsymbol{I}}$. *The parameters* α, λ *and* β *are obtained through the equations:* $\alpha = 1 - \frac{\sigma_y(\bar{\varepsilon}^p)}{q}\left(C_\eta.B.\eta + A.D.\xi\right)$, $\lambda = \frac{3.\sigma_y(\bar{\varepsilon}^p).A.D}{q^2}$ *and* $\beta = \frac{\sigma_y(\bar{\varepsilon}^p)}{q}\left[C_\eta.B - \frac{9.A.D}{2.q^2}\left(tr(\boldsymbol{\sigma}^2) - \frac{tr(\boldsymbol{\sigma})^2}{3}\right)\right]$.

In order to highlight the convergence of the Newton-Raphson algorithm in table 2, we present the relative residual of the solution for two typical load increments when we have both pressure effect and lode angle dependence introduced. The convergence rates, in both of case, are clearly quadratic.

In the figure 2, we can analyze the behavior of the reaction-displacement curve (a) and the accumulated plastic strain-displacement curve (b) obtained numerically. Verifying first the curve reaction-displacement, figure 2(a), the result obtained without

Table 2. *Convergence table for two typical load increments. Flat grooved specimen.*

Iteration number	Relative residual [%]		Iteration number	Relative residual [%]
1	$0.51275\text{x}10^{-2}$		1	$0.17977\text{x}10^{-1}$
2	$0.37416\text{x}10^{-4}$		2	$0.44738\text{x}10^{-3}$
3	$0.21888\text{x}10^{-8}$		3	$0.27548\text{x}10^{-6}$
4	$0.12611\text{x}10^{-14}$		4	$0.10461\text{x}10^{-12}$

including any effect $\left(C_\eta = 0, C^s_\theta = 1, C^t_\theta = 1, C^c_\theta = 1, m = 0\right)$, reproduces the von Mises model. In this case, the error is around 17%, between experimental and numerical results. If only the pressure effect is included $\left(C_\eta = 0.09, C^s_\theta = 1, C^t_\theta = 1, C^c_\theta = 1, m = 0\right)$, the results are similar with Drucker Prager model and the error between the numerical simulation and the experimental one are smaller than the previous case, but still big. In this case, the error is about 13%. Finally, we can introduce both the pressure

Box 2: *The Newton-Raphson algorithm for solution of the return mapping system of equations.*

1) Initialize iteration counter, k: = 0, set initial guess for $\underline{\varepsilon}^{e}_{n+1}{}^{(0)} = \underline{\varepsilon}^{e}_{n}$, $\Delta\gamma^{(0)} = 0$ and $\bar{\varepsilon}^{p}_{n+1}{}^{(0)} = \bar{\varepsilon}^{p}_{n}$ corresponding residual:

$$\begin{bmatrix} r_{\underline{\varepsilon}^{e}_{n+1}}\left(\underline{\boldsymbol{\varepsilon}}^{e}_{n+1}, \Delta\gamma, \bar{\varepsilon}^{p}_{n+1}\right) \\ r_{\Delta\gamma}\left(\underline{\boldsymbol{\varepsilon}}^{e}_{n+1}, \Delta\gamma, \bar{\varepsilon}^{p}_{n+1}\right) \\ r_{\bar{\varepsilon}^{p}_{n+1}}\left(\underline{\boldsymbol{\varepsilon}}^{e}_{n+1}, \Delta\gamma, \bar{\varepsilon}^{p}_{n+1}\right) \end{bmatrix} = \begin{bmatrix} \underline{\boldsymbol{\varepsilon}}^{e}_{n+1} - \underline{\boldsymbol{\varepsilon}}^{e\,trial}_{n+1} + \Delta\gamma . N_{n+1} \\ q_{n+1} - \sigma_y\left(\bar{\varepsilon}^{p}_{n+1}\right) . A_{n+1} . B_{n+1} \\ \bar{\varepsilon}^{p}_{n+1} - \bar{\varepsilon}^{p\,trial}_{n+1} - \Delta\gamma\sqrt{(*)} \end{bmatrix}$$

2) Perform Newton-Raphson iteration

$$\begin{bmatrix} \frac{\partial r_{\underline{\varepsilon}^{e}_{n+1}}}{\partial \underline{\boldsymbol{\varepsilon}}^{e}_{n+1}} & \frac{\partial r_{\underline{\varepsilon}^{e}_{n+1}}}{\partial \Delta\gamma} & \frac{\partial r_{\underline{\varepsilon}^{e}_{n+1}}}{\partial \bar{\varepsilon}^{p}_{n+1}} \\ \frac{\partial r_{\Delta\gamma}}{\partial \underline{\boldsymbol{\varepsilon}}^{e}_{n+1}} & \frac{\partial r_{\Delta\gamma}}{\partial \Delta\gamma} & \frac{\partial r_{\Delta\gamma}}{\partial \bar{\varepsilon}^{p}_{n+1}} \\ \frac{\partial r_{\bar{\varepsilon}^{p}_{n+1}}}{\partial \underline{\boldsymbol{\varepsilon}}^{e}_{n+1}} & \frac{\partial r_{\bar{\varepsilon}^{p}_{n+1}}}{\partial \Delta\gamma} & \frac{\partial r_{\bar{\varepsilon}^{p}_{n+1}}}{\partial \bar{\varepsilon}^{p}_{n+1}} \end{bmatrix}^{k-1} \cdot \begin{bmatrix} \delta\underline{\boldsymbol{\varepsilon}}^{e}_{n+1} \\ \delta\Delta\gamma \\ \delta\bar{\varepsilon}^{p}_{n+1} \end{bmatrix}^{k} = -\begin{bmatrix} r_{\underline{\varepsilon}^{e}_{n+1}}\left(\underline{\boldsymbol{\varepsilon}}^{e}_{n+1}, \Delta\gamma, \bar{\varepsilon}^{p}_{n+1}\right) \\ r_{\Delta\gamma}\left(\underline{\boldsymbol{\varepsilon}}^{e}_{n+1}, \Delta\gamma, \bar{\varepsilon}^{p}_{n+1}\right) \\ r_{\bar{\varepsilon}^{p}}\left(\underline{\boldsymbol{\varepsilon}}^{e}_{n+1}, \Delta\gamma, \bar{\varepsilon}^{p}_{n+1}\right) \end{bmatrix}^{k-1}$$

New guess for $\underline{\boldsymbol{\varepsilon}}^{e}_{n+1}$, $\Delta\gamma$ ***and*** $\bar{\varepsilon}^{p}_{n+1}$***:***

$$\underline{\boldsymbol{\varepsilon}}^{e}_{n+1} = \underline{\boldsymbol{\varepsilon}}^{e}_{n+1}{}^{(k-1)} + \delta\underline{\boldsymbol{\varepsilon}}^{e}_{n+1}{}^{(k)}\,,\quad \Delta\gamma = \Delta\gamma^{(k-1)} + \delta\Delta\gamma^{(k)} \quad \textit{and} \quad \bar{\varepsilon}^{p}_{n+1} = \bar{\varepsilon}^{p}_{n+1}{}^{(k-1)} + \delta\bar{\varepsilon}^{p}_{n+1}{}^{(k)}$$

Update stress tensor:

$$\underline{\boldsymbol{\sigma}}_{n+1} = \mathbf{D}^{e} : \underline{\boldsymbol{\varepsilon}}^{e}_{n+1}\,,\quad p_{n+1} = \frac{1}{3} tr\left(\underline{\boldsymbol{\sigma}}_{n+1}\right) \quad \textit{and} \quad \underline{\boldsymbol{S}}_{n+1} = \underline{\boldsymbol{\sigma}}_{n+1} - p_{n+1}\underline{\boldsymbol{I}}$$

together with other elasto-plastic parameters: q_{n+1}, η_{n+1}, r_{n+1}, ξ_{n+1}, θ_{n+1} and μ_{n+1}

3) Check for convergence

$$\tilde{\Phi} = \tilde{q} - \sigma_y\left(\bar{\varepsilon}^{p}_{n+1}\right) . \left[1 - C_\eta(\eta_{n+1} - \eta_0)\right] . \left[C^{s}_{\theta} + (C^{ax}_{\theta} - C^{s}_{\theta})\left(\mu_{n+1} - \frac{\mu_{n+1}{}^{m+1}}{m+1}\right)\right]$$

IF $\left\|\tilde{\Phi}\right\| \leq \epsilon_{tol}$ THEN RETURN to Box 1.

4) GOTO (*2*)

where, $\tilde{\Phi}$ *and* $\tilde{q}$ *represent the updated yield function and the updated von Mises equivalent stress, respectively, on the discretizated step* t_{n+1}*. The variable* $\bar{\varepsilon}^{p}_{n+1}$ *represents the accumulated plastic strain at* $t = t_{n+1}$*. The variable* $\Delta\gamma$ *represents the plastic multiplier and* σ_y *represents the yield stress for the conventional von Mises model.*

effect and lode angle dependence $\left(C_\eta = 0, C^{s}_{\theta} = 0.855, C^{t}_{\theta} = 1, C^{c}_{\theta} = 0.90, m = 6\right)$. In this case, the reaction-displacement curve agrees well with the experimental results. The error is less than 2%.

By analyzing the accumulated plastic strain-displacement curve, figure 2(b), we can observe the evolution of the accumulated plastic strain as a function of the prescribed displacement. We can verify that only with pressure effect and with both pressure effect and lode angle, the growth rate of the accumulated plastic strain is faster than without effects introduced. In addition, we can conclude that the Bai & Wierzbicki elasto-plastic model reaches higher levels of plastic strain, even for lower levels of equivalent stress, when we have both effects included.

From figure 3, we can determine the point of maximum and minimum equivalent stress for all numerical simulations. For the von Mises model, the maximum equivalent stress attains a value of 900.73 MPa. If only the pressure effect is included, the maximum equivalent stress is equal to 843.35 MPa. When both effects are included, the maximum equivalent stress is equal 721.64 MPa. The maximum value is always located on the central point of

the specimen. The experimental results agree with the numerical simulations when we have the pressure effect and lode dependence introduced.

lation of a flat grooved specimen of the aluminum alloy was used to illustrate the robustness of the proposed algorithm, we verified that both effects

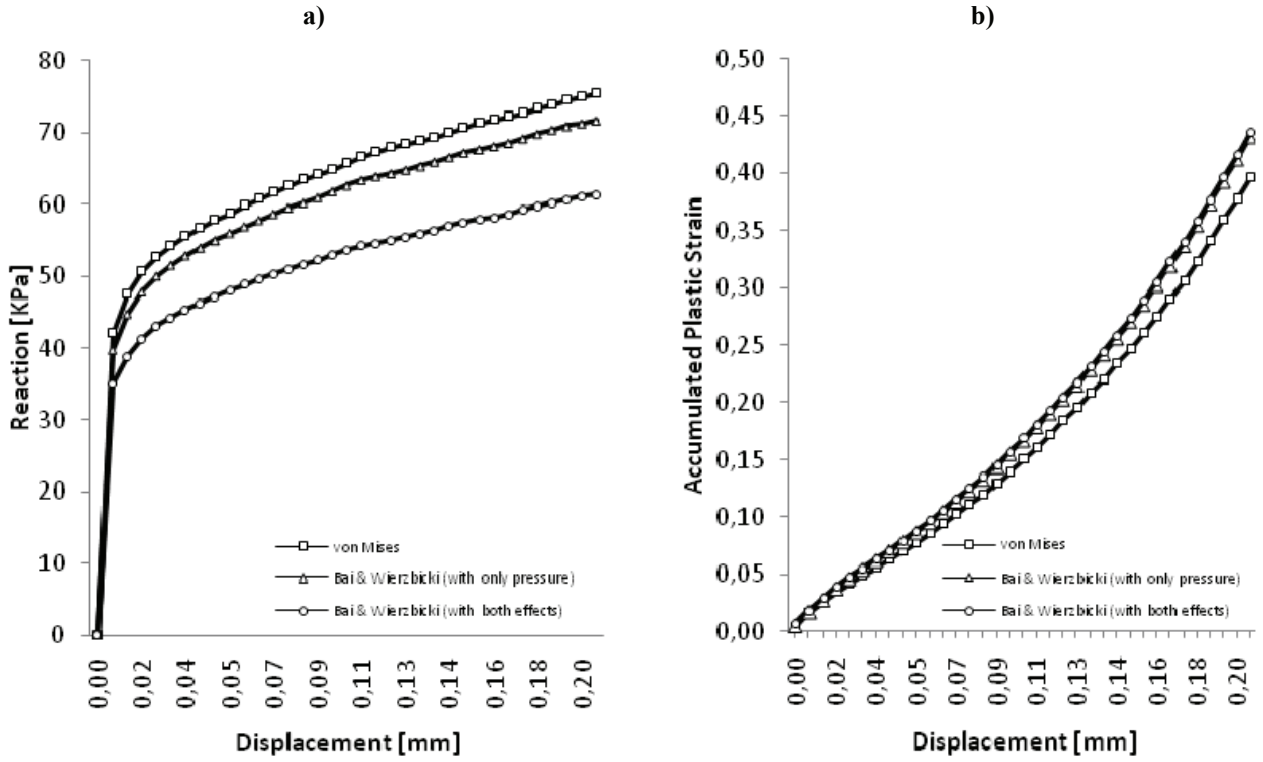

Fig. 2. Reaction-displacement curve (a) and accumulated plastic strain-displacement curve (b) for Bai and Wierzbicki model: without effects (or von Mises model), with only pressure effect included (or Drucker Prager model) and both pressure effect and lode angle dependence included.

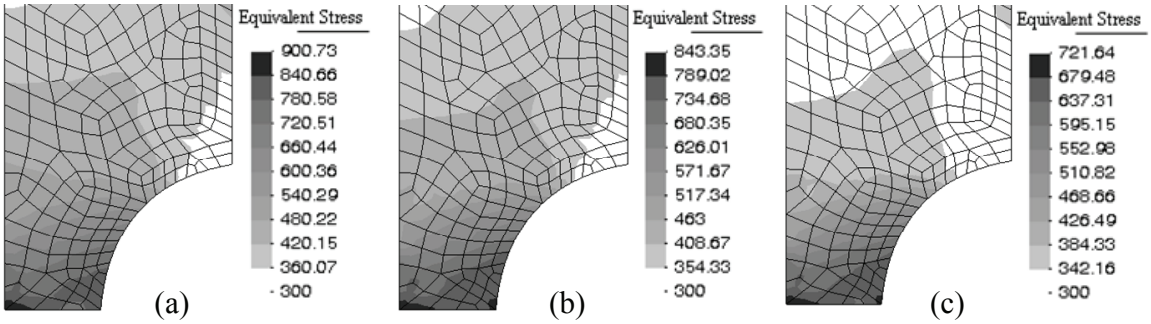

Fig. 3. Equivalent stress parameter plotted through the mesh. (a) without effects or von Mises model, (b) only with pressure effect or Drucker Prager model, and (c) both pressure effect and lode angle dependence.

5. CONCLUSION

In this paper was presented an implicit numerical integration for a recently proposed elasto-plastic model that includes the pressure effect and lode angle dependence into the hardening rule. The convergence of the Newton Raphson algorithm is similar between von Mises model and Bai & Wierzbicki model without effects introduced and between Drucker Prager and Bai & Wierzbicki model with only pressure effect introduced. The numerical simulation of a flat grooved specimen of the aluminum alloy was used to illustrate the robustness of the proposed algorithm, we verified that both effects have to be taken into account on the plastic flow. The error in the reaction-displacement curve for a total displacement of 0.2 [mm] was reduced from 17% to 2% by including both the effect of pressure and lode angle.

REFERENCES

1. Bai, Y., Effect of Loading History on Necking and Fracture, Ph.D Thesis, Massachusetts Institute of Technology, 2008.
2. Bai, Y., Wierzbicki, T., A new model of metal plasticity and fracture with pressure and lode dependence, Int. J. of Plasticity, 2007, doi:10.1016/j.ijplas.2007.09.004.

3. Bao, Y., Predition of Ductile Crack Formation in Uncrecked Bodies, Ph.D Thesis, Massachusetts Institute of Technology, 2003.
4. De Souza Neto, E. A., Peric, D., & Owen, D. R., Computational Methods for Plasticity: Theory and Application. Wiley, 2008.
5. Hill, R., The Mathematical Theory of Plasticity, Oxford Univ. Press, London, 1950.
6. Richmond, O., Spitzig, W.A., Pressure dependence and dilatancy of plastic flow. In Theoretical and Applied Mechanics, Proc. 15th Int. Congress of Theoretical and Applied Mechanics., Toronto, North-Holland Publ Co, Amsterdam, 1980, 377–386.
7. Simo, J., Hughes, T., Computational Inelasticity, Springer, 1998.
8. Wilson, C.D., A critical reexamination of classical metal plasticity, Journal of Applied Mechanics, Transactions ASME, 69(1), 2002, 63–68.

NIEJAWNY ALGORYTM CAŁKOWANIA NUMERYCZNEGO DLA SPRĘŻYSTO-PLASTYCZNEGO MODELU BAI – WIERZBICKIEGO

Streszczenie

Niniejszy artykuł opisuje niejawny algorytm całkowania numerycznego modelu plastyczności i pękania metali. Równania konstytutywne modelu materiału uwzględniają zarówno wpływ ciśnienia przez wprowadzenie współczynnika trójosiowowości i wpływ trzeciego niezmiennika dewiatora tensora naprężenia. Te efekty bezpośrednio wpływają na sposób umacniania się materiału. W pierwszej części artykułu przedstawiono podstawy teoretyczne modelu materiału. Następnie omówione są kroki niezbędne do implementacji modelu w niejawnym quasi-statycznym środowisku elementów skończonych. W szczególności opisane zostały: procedura uaktualniania naprężenia, która opiera się na tak zwanym podziale operatora oferującym standardowy algorytm odwzorowania w stanie sprężystym oraz na procedurze obliczania macierzy stycznych spójnej z uaktualnianiem wartości naprężeń. W końcowej części pracy przedstawiono symulację rozciągania płaskiej próbki z rowkami w celu pokazania wiarygodności i skuteczności proponowanego algorytmu.

Received: October 8, 2007
Received in a revised form: November 6, 2007
Accepted: November 6, 2007